

# The X-ray spectrum of RX J1914.4+2456 revisited

Gavin Ramsay

*Armagh Observatory, College Hill, Armagh, BT61 9DG, Northern Ireland*

Accepted 2007 November 15. Received 2007 November 14; in original form 2007 October 9

## ABSTRACT

It has been proposed that RX J1914.4+2456 is a stellar binary system with an orbital period of 9.5 mins. As such it shares many similar properties with RX J0806.3+1527 (5.4 mins). However, while the X-ray spectrum of RX J0806.3+1527 can be modelled using a simple absorbed blackbody, the X-ray spectrum of RX J1914.4+2456 has proved difficult to fit using a physically plausible model. In this paper we re-examine the available X-ray spectra of RX J1914.4+2456 taken using *XMM-Newton*. We find that the X-ray spectra can be fitted using a simple blackbody and an absorption component which has a significant enhancement of neon compared to the solar value. We propose that the material in the inter-binary system is significantly enhanced with neon. This makes its intrinsic X-ray spectrum virtually identical to RX J0806.3+1527. We re-access the X-ray luminosity of RX J1914.4+2456 and the implications of these results.

**Key words:** Stars: binary - general; abundances; individual: - RX J1914.4+2456, RX J0806.3+1527; X-rays: binaries

## 1 INTRODUCTION

The X-ray source RX J1914.4+2456 (hereafter RX J1914+24) has been the subject of much debate since its discovery during the *ROSAT* all-sky survey. A number of competing models have been put forward to account for its observed properties, but all of them involve a stellar binary system. The models can be split into accretion and non-accretion models. The non-accretion model is the unipolar inductor (UI) model where dissipation of large electrical currents heat the magnetic white dwarf (Wu et al 2002). It shares many similar observational characteristics to the X-ray source RX J0806.3+1527 (hereafter RX J0806+15, see Cropper et al 2004a for a review).

One of the main uncertainties to understanding the nature of RX J1914+24 is accurately determining its X-ray luminosity,  $L_X$ . In the UI model,  $L_X$  is proportional to the rate of change of the orbital period and the degree of asynchronisation between the binary orbital period and the primary star (Wu et al 2002, Dall’Osso et al 2007).

In practise it has been difficult to get an accurate value for  $L_X$ . This is partly due to the fact that RX J1914+24 is highly reddened. The other factor is that its X-ray spectrum is rather unusual and therefore difficult to determine the underlying emission model. X-ray spectra obtained using *XMM-Newton* are not well fitted using a simple absorbed blackbody, showing large residuals near 0.7 keV (Ramsay et al 2005). Ramsay et al (2005) found that an absorbed blackbody with a broad emission line centered at 0.59keV gave

a much improved goodness of fit and for a distance of 1kpc implied  $L_X \sim 10^{35}$  ergs  $s^{-1}$ .

Using two further longer series of observations of RX J1914+24 also taken using *XMM-Newton*, Ramsay et al (2006) found that an absorbed low-temperature thermal plasma model with an edge at 0.83keV gave a significantly improved fit compared to the previous best model fit. For a distance of 1kpc this optically thin emission model gave  $L_X \sim 10^{33}$  ergs  $s^{-1}$ . On the other hand if the distance was much lower than 1 kpc (Steeghs et al 2006, Barros et al 2007) then  $L_X$  could be as low as  $\sim 3 \times 10^{31}$  ergs  $s^{-1}$  – giving a range in  $L_X$  of 4 orders of magnitude!

RX J1914+24 has been observed using *XMM-Newton* at 4 separate epochs (Table 1). An analysis of the data taken using the EPIC detectors have been presented in Ramsay et al (2005) (from the first two epochs) and in Ramsay et al (2006) (from the last two epochs). In this paper we examine the data obtained using the RGS detectors; re-examine the data obtained using the EPIC detectors using more recent calibration data, and also re-examine the models used to fit the data.

## 2 OBSERVATIONS

The data were processed using *XMM-Newton* SAS v7.0 (the data presented previously were processed using v6.0 and v6.5 in Ramsay et al 2005 and Ramsay et al 2006 respectively). In our analysis we excluded time intervals of high

| Revolution | Date of Observation | EPIC PN |          | EPIC MOS1 |          | EPIC MOS2 |          | RGS      | Flux                                  |
|------------|---------------------|---------|----------|-----------|----------|-----------|----------|----------|---------------------------------------|
|            |                     | Mode    | Duration | Mode      | Duration | Mode      | Duration | Duration | ergs s <sup>-1</sup> cm <sup>-2</sup> |
| 0718       | 2003-11-09          | sw      | 6641     | timing    | 8933     | sw        | 8993     | 9880     | $1.25 \times 10^{-12}$                |
| 0721       | 2003-11-15          | sw      | 2888     | timing    | 3865     | sw        | 3865     | 4000     | $1.20 \times 10^{-12}$                |
| 0880       | 2004-09-28          | ff      | 11869    | ff        | 14954    | ff        | 14954    | 16954    | $1.27 \times 10^{-12}$                |
| 0882       | 2004-10-02          | ff      | 15274    | ff        | 18419    | ff        | 18419    | 18880    | $1.40 \times 10^{-12}$                |

**Table 1.** The log for the observations of RX J1914+24 made using *XMM-Newton*. We show the mode the detector was in where ‘sw’ refers to ‘small window’, ‘ff’ to ‘full frame’ and the duration of ‘good’ time – ie excluding time intervals of enhanced background. The RGS detectors were configured in ‘Spectroscopy’ mode. In the last column we show the observed integrated flux in the 0.2–10keV energy band using the EPIC pn detector data and fitting an absorbed blackbody plus broad emission line spectral model.

particle/solar background (a significant issue in the second epoch observation).

For those observations when the EPIC data were in full frame mode, we excluded events from the central core of the psf (using an aperture of  $10''$  in radius) in order that pile-up was not significant. We did not extract spectra from the timing mode data since the spectral calibration is not as well defined as for the other modes. For the RGS data, we extracted spectra which included the source and background, and a background spectrum separately. We grouped the EPIC spectra so that each bin had a minimum of 40 counts. Since the RGS spectra from the individual epochs were relatively low, we co-added the spectra from the RGS1 and RGS2 detectors obtained using the 3rd and 4th epoch observations (the first two epochs had much shorter exposures). We used the *SAS* task `rgscombine` and then grouped each spectrum so that each bin of each spectrum had a minimum of 20 counts per bin.

To determine the observed X-ray flux at each epoch, we used data taken using the EPIC pn detector. We fitted the integrated X-ray spectra using an absorbed blackbody plus broad emission line. We show the integrated observed flux in the 0.2–10keV energy band using in Table 1 (the observed flux is only weakly sensitive to the model used). This shows that the observed flux varied by 17% between the 4 observation epochs.

The X-ray data folded on the 569 sec period shows a distinctive ‘on-off’ behaviour, with the X-ray flux being off for approximately half the 569 sec period (Cropper et al 1998). There is a sharp rise in flux which is followed by a slower decline from maximum brightness. Ramsay et al (2005) showed evidence using the two shorter duration observations that the spectrum gets softer during this decline phase. Using the 3rd and 4th longer series of observations we confirm this finding. Therefore we have obtained a spectrum which covers the ‘bright phase’ which we define to be  $\phi=0.08-0.38$  where  $\phi=0.0$  is defined as the start of the sharp rise in X-ray flux.

### 3 THE RGS SPECTRA

We extracted RGS spectra from the bright phase using the 3rd and 4th epoch observations. In fitting the spectra, we used a blackbody, a blackbody plus a Gaussian component both in absorption and emission and a multi-temperature thermal plasma plus edge model. In the work of Ramsay et al (2005, 2006), the absorption model which was used was

| Model            | $\chi^2_\nu$<br>(dof) |
|------------------|-----------------------|
| tbabsvmekaledge  | 2.18 (93)             |
| tbabsbb          | 2.12 (95)             |
| tbvarabsbb       | 1.28 (93)             |
| tbabsbbgau (abs) | 1.20 (92)             |
| tbabsbbgau (emi) | 1.14 (91)             |

**Table 2.** The fits to the bright phase RGS spectrum taken from data in *XMM-Newton* orbits 0880 and 0882. The models noted in the first column refer to the models in *XSPEC*: tbabs – Tübingen Boulder absorption ISM model (Wilms et al 2000); tbvarabs – Tübingen Boulder absorption ISM model with variable abundances; bb – blackbody; gau – a Gaussian component in emission (emi) and absorption (abs); vmekal – a thermal plasma model with non-solar abundances; edge - an absorption edge; In the second column we show the  $\chi^2_\nu$  and (degrees of freedom).

the ‘wa’ neutral absorption model found in the *XSPEC* fitting package (Arnaud 1996). Here, we use the Tübingen–Boulder absorption ISM model and abundances (Wilms, Allen & McCray 2000) which incorporates advances in atomic cross-sections and other physical parameters compared to the wa model (Morrison & McCammon 1983). We used this model implemented into *XSPEC* as the `tbabs` model (which assumes an interstellar medium of solar abundance) and the `tbvarabs` model (which allows the abundance of each element to vary).

We show the goodness of fit to the RGS spectrum using the different models in Table 2. As was found by Ramsay et al (2005) a simple absorbed blackbody model gives a very poor fit. Ramsay et al (2006) found that a low temperature thermal plasma plus edge model gave a good fit to the spectrum obtained using the EPIC pn detector. Using the RGS data we can rule this model out. The temperature of the plasma determined using the EPIC pn detector is very low, ( $< 1\text{keV}$ ), which would result in strong X-ray emission lines – these lines are not detected in the RGS data.

This leaves three models – a blackbody with either an absorption or emission component, or a blackbody with an absorption component which has abundance different to solar composition. We show the RGS spectrum together with the best fit using an absorbed blackbody, where the absorption component has variable abundances, in Figure 1.

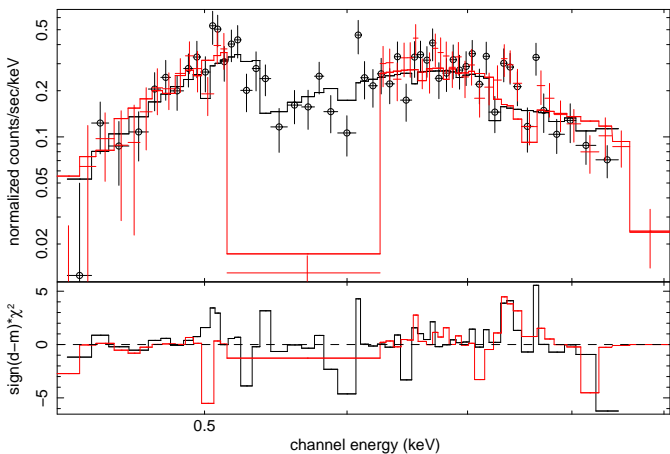


**Figure 1.** The fits to the RGS spectra bright phase spectra. The spectra from each detector (RGS1 - datapoints plotted as black circles, RGS2 red points) taken in the 3rd and 4th epoch observations. The solid lines show the best fit using an absorbed blackbody model (the darker line through the RGS1 data and lighter, or red, line for the RGS2 data), where the absorption component has variable abundances.

#### 4 THE EPIC PN BRIGHT PHASE SPECTRA

We extracted bright phase spectra from each epoch. We fitted models consisting of a blackbody and a Gaussian line in both emission and absorption, and also a blackbody with an absorption component with variable abundances. We show the goodness of fits to these spectra using these three models in the top panel of Table 3. (For the second epoch observation, which had a short good exposure we fixed the model parameters at the best fit parameters determined in fourth observation apart from the absorption column density and the normalisation parameters). We find that the models which include a Gaussian in absorption or emission give formally good fits (95 % confidence) while the model with an interstellar component with variable interstellar abundance gives a  $\chi^2_{\nu} \leq 1.0$ .

We show the observed flux in the 0.2–10keV energy band and also the unabsorbed flux in the 0.01–10keV energy band in the bottom panel of Table 3. The observed flux at each epoch as derived from the various models is consistent to within 7%. In contrast, the derived unabsorbed flux varies by more than an order of magnitude.

We show the spectral parameters derived for the blackbody plus a Gaussian component in Table 4. The spectral parameters derived using a blackbody plus Gaussian line in emission gives consistent results, with a blackbody temperature  $kT \sim 62$  eV and  $N_H \sim 5 \times 10^{21}$  cm<sup>-2</sup>. The center of the Gaussian component is  $\sim 0.65$  keV and has a width  $\sim 80$  eV and an equivalent width  $\sim 160$  eV. In contrast, the spectral parameters as derived using the model with the Gaussian line in absorption, show a greater spread. However, the temperature of the blackbody component is hotter than in the previous model. The center of the absorption line is  $\sim 0.86$  keV and has a width  $\sim 0.11$  keV.

Since the variable abundance absorption model was not used by Ramsay et al (2005, 2006) we now go onto investigate this model in more detail. We fit the spectra using

an absorbed blackbody model where we allowed the abundance of the absorbing material to vary from solar. We did this by allowing each element to vary from solar one at a time. If there was no significant change in the goodness of fit, we re-set the abundance for that element back to solar and fixed this parameter. We did this for the EPIC pn and RGS spectra from *XMM-Newton* orbits 0880 and 0882 individually. We show the spectral parameters for these fits in Table 5. We find that their X-ray spectra can be well fitted using blackbody with an interstellar absorption model which has significantly increased amounts of Neon. There is some evidence that Iron could have non-solar abundances.

We also fitted the EPIC pn spectra taken from *XMM-Newton* orbits 0718 and 0721 using this same model. As mentioned before, for the data taken in the orbit 0721 observations, we fixed the spectral parameters at their best fit parameters determined in orbit 0882 (apart from the absorption column density and the blackbody normalisation). We show the spectral parameters derived from these spectra in Table 5. We find these spectra are also consistent with the abundance of neon being significantly enhanced in these epochs as well.

#### 5 AN EVALUATION OF THE SPECTRAL MODELS

We now go onto to discuss the physical plausibility of the three spectral models which we have used. Namely, the absorbed blackbody with an absorption component and an emission component, and the blackbody with absorption component with non-solar abundances.

##### 5.1 A blackbody with Gaussian absorption component

Isolated neutron stars (INS) with high magnetic fields have been found to show absorption lines which have been attributed to either a proton cyclotron line or an electron cyclotron line, see Zane et al (2005), Haberl (2007) and Schwöpe et al (2007). The similarity between the spectral parameters of RX J1914+24 and some INS is quite striking. For instance, the width of the line and its equivalent width as measured in RX J1914+24 is very similar to that of RBS 1223 (Schwöpe et al 2007). Also the variation in the observed flux in the energy range 0.35–1.5keV of the INS RX J0720.4–3125 is 20% (cf 17 % between the *XMM-Newton* observations of RX J1914+24) showing that non-accreting sources can show a significant variation in their X-ray flux (the data on RX J0720.4–3125 were extracted from the *XMM-Newton* archive).

There are, however, some very significant differences between the observed properties of RX J1914+24 and that of INS. The first is that their spin-periods are in the range  $\sim 3 - 12$  sec - these are very much shorter than the period seen in RX J1914+24 (569 sec). The second is the luminosity difference - INS show X-ray luminosities  $\lesssim 10^{31}$  ergs s<sup>-1</sup>. Using the inferred unabsorbed fluxes as derived using the blackbody plus Gaussian absorption line, we find that RX J1914+24 would have to be at a distance of 20 pc to give a comparable luminosity. If RX J1914+24 was so close, we would expect to detect a significant proper motion which

| Model            | 0718                   |                        | 0721                   |                        | 0880                   |                        | 0882                   |                        |
|------------------|------------------------|------------------------|------------------------|------------------------|------------------------|------------------------|------------------------|------------------------|
|                  | Flux <sup>o</sup>      | Flux <sup>u</sup>      | Flux <sup>o</sup>      | Flux <sup>u</sup>      | Flux <sup>o</sup>      | Flux <sup>u</sup>      | Flux <sup>o</sup>      | Flux <sup>u</sup>      |
| tbabsbbgau (emi) | $8.24 \times 10^{-12}$ | $7.35 \times 10^{-10}$ | $8.75 \times 10^{-12}$ | $8.80 \times 10^{-10}$ | $3.45 \times 10^{-12}$ | $2.60 \times 10^{-10}$ | $3.62 \times 10^{-12}$ | $6.19 \times 10^{-10}$ |
| tbabsbbgau (abs) | $8.54 \times 10^{-12}$ | $1.82 \times 10^{-10}$ | $8.97 \times 10^{-12}$ | $2.20 \times 10^{-10}$ | $3.50 \times 10^{-12}$ | $2.68 \times 10^{-10}$ | $3.63 \times 10^{-12}$ | $2.42 \times 10^{-10}$ |
| tbvarabsbb       | $8.27 \times 10^{-12}$ | $2.90 \times 10^{-9}$  | $8.73 \times 10^{-12}$ | $1.80 \times 10^{-9}$  | $3.49 \times 10^{-12}$ | $3.38 \times 10^{-10}$ | $3.62 \times 10^{-12}$ | $1.34 \times 10^{-9}$  |

**Table 3.** Top panel: The fits to the bright phase EPIC pn spectrum obtained using *XMM-Newton* at four epochs. The models noted in the first column are defined in the caption for Table 2. In the following columns we show the goodness of fit ( $\chi^2_\nu$  and degrees of freedom). Bottom panel: we show the observed flux, Flux<sup>o</sup>, in the 0.2–10keV energy band, and the implied unabsorbed flux, Flux<sup>u</sup>, in the 0.01–10keV energy band for all four epochs and the three spectral models.

| <i>XMM</i><br>Orbit              | $N_{\text{H}}$<br>( $10^{21} \text{ cm}^{-2}$ ) | $kT_{bb}$<br>(eV)      | E<br>(keV)             | $\sigma$<br>(keV)         | EW<br>(eV)          |
|----------------------------------|---|------------------------|------------------------|---------------------------|---------------------|
| Gaussian component in emission   |   |                        |                        |                           |                     |
| 0718                             | $4.2^{+0.5}_{-0.7}$                             | $64.9^{+1.9}_{-4.6}$   | $0.64^{+0.02}_{-0.03}$ | $0.075^{+0.018}_{-0.014}$ | $182^{+104}_{-55}$  |
| 0880                             | $5.7^{+0.1}_{-0.2}$                             | $57.5^{+1.8}_{-2.0}$   | $0.63 \pm 0.01$        | $0.093^{+0.004}_{-0.005}$ | $152^{+15}_{-20}$   |
| 0882                             | $5.1^{+0.1}_{-0.7}$                             | $63.9^{+1.1}_{-4.7}$   | $0.68 \pm 0.01$        | $0.06^{+0.02}_{-0.01}$    | $147^{+61}_{-26}$   |
| Gaussian component in absorption |   |                        |                        |                           |                     |
| 0718                             | $2.9^{+0.3}_{-0.2}$                             | $110^{+18}_{-10}$      | $0.86^{+0.02}_{-0.47}$ | $0.111^{+0.006}_{-0.006}$ | $-216^{+53}_{-247}$ |
| 0880                             | $4.9^{+0.7}_{-0.7}$                             | $80.7^{+17.7}_{-10.2}$ | $0.87^{+0.04}_{-0.10}$ | $0.12^{+0.03}_{-0.03}$    | $-148^{+64}_{-226}$ |
| 0882                             | $6.2^{+0.5}_{-0.9}$                             | $70.6^{+6.2}_{-2.2}$   | $0.84^{+0.02}_{-0.09}$ | $0.105^{+0.03}_{-0.02}$   | $-104^{+39}_{-134}$ |

**Table 4.** The spectral parameters for fits to the bright phase spectra using an absorbed blackbody model where we have allowed the abundance of the absorption component to vary from solar. The duration of the EPIC pn spectrum from *XMM-Newton* orbit 0721 was relatively short and hence the spectral parameters are not strongly constrained.

has not been observed (Israel et al 2002). The third difference is the change in the period. The 569 sec period in RX J1914+24 has been found to be decreasing, while the period of the two INS which have been found to show a change in their period are increasing (Cropper et al 2004b, Kaplan & van Kerkwijk 2005a, Kaplan & van Kerkwijk 2005b). A fourth difference is the optical brightness, with INS being typically  $B \sim 26$  (see the compilation in Haberl 2007), while RX J1914+24 is  $B \sim 21$ . We conclude RX J1914+24 is not an isolated neutron star. At this point, whilst we cannot rule out the presence of absorption features in the X-ray spectrum of RX J1914+24, we do not consider it the most likely model to explain its X-ray spectrum.

## 5.2 A blackbody with Gaussian emission component

A blackbody with an additional broad emission line does, on first sight, seem rather contrived. However, such a feature has been claimed to be present in the relatively low resolution *ASCA* spectra of a number of X-ray ultra-compact binaries with neutron star primaries (eg Juett, Psaltis & Chakrabarty 2001). The line center of the emission line is remarkably similar in RX J1914+24 and the four sources

shown described in Juett et al (2001). One notable difference is that the temperature of the blackbody component in the X-ray UCBs is much hotter – several hundred eV as opposed to  $\sim 60$  eV – and the fact that they are hard X-ray sources being detected at energies up to many 10’s of keV. This is the result of the primary being a neutron star as opposed to a white dwarf.

It was claimed that this broad emission feature was due to the superposition of a number of unresolved emission lines. However, when one of the sources observed using *ASCA* was observed using the *Chandra* Low Energy Grating Spectrometer, it failed to detect any emission features which could give rise to a broad emission feature in low resolution spectra. We now address one possible reason for this.

## 5.3 A blackbody with variable abundances in the absorption model

Juett et al (2001) found that good fits to *Chandra* spectra of neutron star UCBs were obtained if the absorption model had non-solar abundances. In particular, they found a high relative abundance of neon and suggested that this overabundance was located in the inter-binary system. However, further work (eg Juett & Chakrabarty 2005) showed that for

| XMM Orbit | Detector | $N_{\text{H}}$<br>( $\text{cm}^{-2}$ ) | $kT_{\text{bb}}$<br>(eV) | N<br>( $Z_{\odot}$ ) | Ne<br>( $Z_{\odot}$ ) | Fe<br>(dof)         | $\chi^2_{\nu}$ |
|-----------|----------|--|--------------------------|----------------------|-----------------------|---------------------|----------------|
| 0718      | pn       | $6.1^{+0.2}_{-0.2}$                    | $65^{+13}_{-9}$          |                      | $9.5^{+1.9}_{-1.5}$   |                     | 0.90 (50)      |
| 0721      | pn       | $5.6^{+0.3}_{-0.3}$                    | 65                       | 0.02                 | 7.8                   | 0.0                 | 0.84 (22)      |
| 0880      | pn       | $4.3^{+1.4}_{-1.0}$                    | $72^{+12}_{-8}$          |                      | $20^{+12}_{-7}$       |                     | 1.00 (72)      |
| 0880      | rgs      | $3.6^{+1.0}_{-0.6}$                    | $67^{+7}_{-5}$           |                      | $39_{-4}$             | $2.6^{+1.0}_{-0.9}$ | 1.09 (162)     |
| 0882      | pn       | $6.8^{+0.2}_{-0.1}$                    | $65^{+9}_{-5}$           | < 0.43               | $7.8^{+1.1}_{-1.0}$   | < 0.26              | 0.88 (88)      |
| 0882      | rgs      | $5.2^{+1.4}_{-1.1}$                    | $66^{+4}_{-4}$           |                      | $20^{+3}_{-5}$        |                     | 1.03 (192)     |

**Table 5.** The spectral parameters for fits to the bright phase spectra using an absorbed blackbody model where we have allowed the abundance of the absorption component to vary from solar. Since the duration of the spectrum taken in orbit 0721 was short, the spectral parameters were fixed at their values determined in orbit 0882 apart from the total absorption column density and normalisation of the blackbody component.

individual sources, the Ne/O ratio showed evidence for variability from epoch to epoch, which they attributed to source variability. This implied that the abundances could not be used to determine the composition of the mass donating star.

There is a clear similarity between the neutron star UCBs described by Juett et al and RX J1914+24. In each observation of RX J1914+24, there is clear evidence that the absorption component has an overabundance of neon.

## 6 DISCUSSION

For the reasons outlined in §5.1, we rule out RX J1914+24 being an isolated neutron star. Since all the known neutron star UCBs have X-ray emission extending up to many 10's of keV we also rule out an accreting neutron star UCB model. We cannot rule out that a neutron star is in a binary system where a secondary star was not filling its Roche Lobe. In this scenario, an X-ray bright system would have to be powered by UI.

It is highly unlikely that the line of sight absorption to RX J1914+24 has a chance enhancement of neon. It is much more likely that this overabundance is concentrated in the binary system. Juett & Chakrabarty (2005) noted that for some neutron star UCBs the Ne/O abundance varied from epoch to epoch and hence the observations could not be used to determine the abundance of the secondary, mass-donating star, in the binary system. In the case of RX J1914+24 there is clear evidence for a significant over-abundance of neon in the absorption component at each epoch. At this stage it is not clear if this over-abundance is due to circumbinary material left over from a previous stage in the binary formation process or can give us a direct insight into the chemical composition of the secondary star (if accretion is occurring).

What are the implications of our findings regarding the X-ray luminosity of RX J1914+24? Steeghs et al (2006) discuss the extinction and distance estimates to RX J1914+24. While the distance is rather uncertain, it is likely that it is greater than  $\sim 1$  kpc. We can rule out the lower estimates ( $L_X \sim 10^{33}$  ergs  $\text{s}^{-1}$  for a distance of 1 kpc) which were derived using a low temperature thermal plasma model. Taking the unabsorbed bolometric fluxes derived using the blackbody with absorption component with variable abun-

dances and assuming a distance of 1 kpc we find  $L_X = 2 \times 10^{34} - 1.6 \times 10^{35}$  ergs  $\text{s}^{-1}$ .

Dall'Osso et al (2007) made a detailed investigation of the UI model in the context of RX J1914+24 and RX J0806+15. They predicted that for low luminosities,  $L_X \sim 10^{33}$  ergs  $\text{s}^{-1}$ , the asynchronism between the orbit and the magnetic star in RX J1914+24 would have to be  $\alpha \sim 0.9-0.98$ , where  $\alpha = \omega_1/\omega_o$ , and  $\omega_1$  is the rotation frequency of the primary star and  $\omega_o$  is the orbital frequency. Unless RX J1914+24 was located at a distance significantly less than 1kpc, we can rule these low values of asynchronism. For high luminosities ( $L_X = 10^{34-35}$  ergs  $\text{s}^{-1}$ ), Dall'Osso et al (2007) predicted that an asynchronism of a few was required ( $\alpha \sim 4$ ). For an observed period of 569 sec,  $\alpha = 2-10$  gives a predicted period of  $\sim 60-300$  sec. There is no evidence for power at these periods in the power spectra of the X-ray light curves (Ramsay et al 2006).

## 7 SUMMARY

Until now the nature of the emission source that powers the X-ray spectrum of RX J1914+24 has been far from clear. In this paper we have shown that it can be well modelled using a simple blackbody model with an absorption component which has non-solar abundances, in particular, an enhancement of neon.

Since the X-ray light curves of RX J1914+24 and RX J0806+15 are practically identical, it suggests that their X-ray emission source is the same. The fact that their X-ray spectra were apparently different (albeit both being soft) was therefore perplexing. Our result showing that the emission source is the same for both RX J1914+24 and RX J0806+15 is therefore very attractive. Indeed their temperatures are virtually identical – we obtain a mean value of  $kT \sim 67$  eV for RX J1914+24 compared to  $kT \sim 65$  eV for RX J0806+15 (Israel et al 2003).

The difference between the X-ray spectrum of RX J1914+24 and RX J0806+15 is that the absorption component of RX J1914+24 has enhanced neon abundance. A further investigation of the optical spectrum of RX J1914+24 to search for neon features is strongly encouraged.

## 8 ACKNOWLEDGEMENTS

I will wish to thank Mark Cropper, Pasi Hakala and Peter Wheatley for useful discussions. Armagh Observatory is grant aided by the N. Ireland Dept. of Culture, Arts and Leisure.

## REFERENCES

- Arnaud, K. A., 1996, *Astronomical Data Analysis Software and Systems V*, eds Jacoby, G., Barnes, J., p17, ASP Conf Series, 101
- Barros, S. C. C., Marsh, T. R., Dhillon, V. S., Groot, P. J., Littlefair, S., Nelemans, G., Roelofs, G., Steeghs, D., Wheatley, P. J., 2007, *MNRAS*, 374, 1334
- Cropper, M., Harrop-Allin, M. K., Mason, K. O., Mittaz, J. P. D., Potter, S. B., Ramsay, G., 1998, *MNRAS*, 293, L57
- Cropper, M., Ramsay, G., Wu, K., Hakala, P., 2004a, In Proc ‘Magnetic Cataclysmic Variables’, IAU Colloquium 190, ASP Conference Proceedings, Vol. 315., p324
- Cropper, M., Haberl, F., Zane, S., Zavlin, V. E., 2004b, *MNRAS*, 351, 1099
- Dall’Osso, S., Israel, G. L., Stella, L., 2007, *A&A*, 464, 417
- Haberl, F., 2007, *Ap&SS*, 308, 181
- Juett, A. M., Psaltis, D., Chakrabarty, D., 2001, *ApJ*, 560, L59
- Juett, A. M., Chakrabarty, D., 2005, *ApJ*, 627, 926
- Israel, G. L., 2002, *A&A*, 386, L13
- Israel, G. L., 2003, *ApJ*, 598, 492
- Kaplan, D. L., van Kerkwijk, M. H., 2005a, *ApJ*, 628, L45
- Kaplan, D. L., van Kerkwijk, M. H., 2005b, *ApJ*, 635, L65
- Morrison, R., McCammon, D., 1983, *ApJ*, 270, 119
- Ramsay, G., Hakala, P., Wu, K., Cropper, M., Mason, K. O., Córdova, F. A., Friedhorsky, W., *MNRAS*, 2005, 357, 49
- Ramsay, G., Cropper, M., Hakala, P., 2006, *MNRAS*, 367, L62
- Schwöpe, A. D., Hambaryan, V., Haberl, F., Motch, C., 2007, *Ap&SS*, 308, 619
- Steenhals, D., Marsh, T. R., Barros, S. C. C., Nelemans, G., Groot, P. J., Roelofs, G. H. A., Ramsay, G., Cropper, M., 2006, *ApJ*, 649, 382
- Wilms, J., Allen, A., McCray, R., 2000, *ApJ*, 542, 914
- Wu, K., Cropper, M., Ramsay, G., Sekiguchi, K., 2002, *MNRAS*, 331, 221
- Zane, S., Cropper, M., Turolla, R., Zampieri, L., Chierigato, M., Drake, J. J., Treves, A., 2005, *ApJ*, 627, 397